Journal of Power Sources 238 (2013) 157–164

Contents lists available at SciVerse ScienceDirect

Journal of Power Sources

journal homepage: www.elsevier.com/locate/jpowsour

Highly dispersed Pt nanoparticles supported on manganese oxide–poly(3,4-ethylenedioxythiophene)–carbon nanotubes composite for enhanced methanol electrooxidation

Lu Wei, You-Jun Fan*, Jing-Hua Ma, Liu-Hong Tao, Rui-Xiang Wang, Jing-Ping Zhong, Hui Wang

Key Laboratory for the Chemistry and Molecular Engineering of Medicinal Resources, Ministry of Education of China, College of Chemistry and Chemical Engineering, Guangxi Normal University, Guilin 541004, China

HIGHLIGHTS

- A new Pt-based catalyst using the MnO_x–PEDOT–MWCNTs composite as support is reported.
- Highly dispersed Pt nanoparticles are uniformly deposited on the MnO_x–PEDOT–MWCNTs.
- The catalyst shows high catalytic performance for methanol oxidation reaction (MOR).

GRAPHICAL ABSTRACT

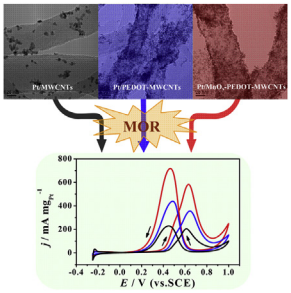

ARTICLE INFO

Article history:
Received 29 December 2012
Received in revised form
10 March 2013
Accepted 12 March 2013
Available online 26 March 2013

Keywords:
Platinum
Manganese oxide
Poly(3,4-ethylenedioxythiophene)
Carbon nanotubes
Methanol electrooxidation

ABSTRACT

We herein report a novel Pt-based electrocatalyst for direct methanol fuel cells (DMFCs) using multi-walled carbon nanotubes (MWCNTs) supported manganese oxide and poly(3,4-ethylenedioxythiophene) (PEDOT) nanocomposite (MnO_x–PEDOT–MWCNTs) as catalyst support for Pt nanoparticles. The prepared nanocomposites are characterized by Fourier transform infrared (FTIR) spectroscopy, X-ray diffraction (XRD), transmission electron microscopy (TEM), X-ray photoelectron spectroscopy (XPS) and electrochemical tests. The results demonstrate that Pt nanoparticles are uniformly deposited on the surface of MnO_x–PEDOT–MWCNTs, and their dispersion and electrochemical active surface area (ECSA) are obviously improved. The methanol electrooxidation activity and stability of the Pt/MnO_x–PEDOT–MWCNTs are significantly enhanced as compared with the Pt/PEDOT–MWCNTs and Pt/MWCNTs catalysts. This study implies that the as-prepared Pt/MnO_x–PEDOT–MWCNTs will be a promising candidate as an anode electrocatalyst in DMFCs.

1. Introduction

In the past decades, direct methanol fuel cells (DMFCs) have received extensive attention due to their simplicity, easy handle, low operating temperature, high energy density and potential applications as green and portable power sources [1–4]. However, one of the major challenges for DMFCs commercialization is the production of low-cost electrocatalysts with high catalytic activity and long-term durability. Up to now, Pt-based electrocatalysts have been widely used as the anode electrode materials for methanol oxidation, but the poor Pt utilization and significantly high costs of the catalysts remain unresolved. It is well known that the utilization ratio of noble metal Pt is closely interrelated with its dispersion and electrochemical active surface area (ECSA) [5]. In order to

* Corresponding author. Tel.: +86 773 5846279; fax: +86 773 2120958.
E-mail address: youjunfan@mailbox.gxnu.edu.cn (Y.-J. Fan).

0378-7753/$ – see front matter © 2013 Elsevier B.V. All rights reserved.
http://dx.doi.org/10.1016/j.jpowsour.2013.03.051

disperse Pt and to get high ECSA, many efforts have been devoted to changing the support materials and their surface condition [6–8]. Recently, it has been found that the composites consisting of a combination of both conducting polymers and carbon nanotubes (CNTs) are the promising support materials, which can obviously improve the dispersion of Pt-based nanoparticles, and thus enhance the electrochemical performance of the catalysts [9–13]. For instance, Selvaraj et al. [10] prepared the Pt/PPy–CNTs and PtRu/PPy–CNTs catalysts with higher methanol electrooxidation activity by depositing well dispersed Pt or PtRu nanoparticles on the polypyrrole (PPy)–CNTs composites. Qu et al. [13] reported the synthesis of Pt/PPy–multi-walled carbon nanotubes (MWCNTs) composite catalyst by a $NaBH_4$ reduction method, which exhibited better electrocatalytic stability than the Pt/MWCNTs catalyst. It is noteworthy that, among various conducting polymers, Poly(3,4-ethylenedioxythiophene) (PEDOT) has been of great interest owing to its high conductivity, remarkable stability, very good film forming properties and high compatibility with other materials [14,15]. Especially, several research groups have focused on exploring the PEDOT–CNTs composites for the energy storage applications [16–20]. Wang et al. [17] synthesized the PEDOT-functionalized single-walled carbon nanotubes composite with greater specific capacitance (200 F g^{-1}). Sharma et al. [19] fabricated a MWCNT–PSS/PEDOT/MnO_2 nanocomposite, which exhibited much higher specific capacitance (375 F g^{-1}) than the MWCNT–PSS/MnO_2 (175 F g^{-1}) and MWCNT–PSS (15 F g^{-1}) nanocomposites. Nevertheless, less attention has been paid so far to employ this kind of composites as the dispersion medium for Pt-based nanoparticles.

On the other hand, it is found that certain metal oxides, such as RuO_2 [5,21], CeO_2 [22–24], SnO_2 [25], V_2O_5 [26], MgO [27] and WO_3 [28], can promote the activity and CO-poisoning tolerance of Pt-based catalysts for alcohol electrooxidation through synergetic interaction with Pt. In recent years, manganese oxide (MnO_x) has attracted more and more attention, and become widely used to store and convert charges in electrochemical supercapacitors [19,29–33]. Moreover, MnO_x was also used as a co-catalytic material of DMFCs to improve the methanol oxidation activity by some researchers [34,35]. However, the poor electric conductivity of single MnO_x restricts its practical applications as the electrode materials [32]. To overcome this weakness, binary or ternary composites of MnO_x with other materials such as CNTs [33–36], graphene [29,37] or conducting polymers [19,30,32], have been explored and demonstrated improvement in the electrochemical performance. Zhou et al. [34] synthesized the Pt/MnO_2/CNTs and PtRu/MnO_2/CNTs nanocatalysts by loading hydrous MnO_2 and Pt (or PtRu alloy) nanoparticles on CNTs, which could effectively enhance the electrooxidation activity of methanol as compared to Pt/CNTs and PtRu/CNTs.

In this work, a novel Pt/MnO_x–PEDOT–MWCNTs composite catalyst is fabricated for the methanol electrooxidation. In this method, the ternary MnO_x–PEDOT–MWCNTs supports are prepared by one step co-deposition of PEDOT and MnO_x on the MWCNTs surface, followed by the deposition and reduction of highly dispersed Pt nanoparticles on the MnO_x–PEDOT–MWCNTs supports. The prepared nanocomposites were characterized by Fourier transform infrared (FTIR) spectroscopy, X-ray diffraction (XRD), transmission electron microscopy (TEM), energy dispersive X-ray (EDX) spectroscopy and X-ray photoelectron spectroscopy (XPS). The electrocatalytic activity and durability of the Pt/MnO_x–PEDOT–MWCNTs catalyst were evaluated by cyclic voltammetry (CV) and chronoamperometry methods. The results show that the Pt/MnO_x–PEDOT–MWCNTs has smaller particle size and better dispersion of Pt nanoparticles and show a much higher electrocatalytic activity and stability for the methanol oxidation reaction, in comparison with the Pt nanoparticles supported on acid-treated MWCNTs.

2. Experimental

2.1. Materials

The raw MWCNTs were purchased from Shenzhen Nanotech Port Co. Ltd. (Shenzhen, China) with the diameter of 40–60 nm, length of 5–15 μm, and purity of 98%. 3,4-ethylenedioxythiophene (EDOT) and 5 wt% Nafion solution were purchased from Sigma–Aldrich. Sodium dodecyl sulfate (SDS), $Mn(CH_3COO)_2 \cdot 4H_2O$, $KMnO_4$, $H_2PtCl_6 \cdot 6H_2O$, $NaBH_4$, $FeCl_3$, $K_2C_2O_4$, methanol, sulfuric acid, nitric acid, acetic acid and sodium acetate were obtained from Sinopharm Chemical Reagent Co. Ltd (Shanghai, China). All chemical reagents used in this experiment were of analytical grade and used as received without further purification. All aqueous solutions were prepared using tridistilled water.

2.2. Preparation of composite catalysts

MWCNTs were at first treated by a conventional acid oxidation method to introduce oxygenous groups that increase the surface activity of MWCNTs. Briefly, 100 mg of raw MWCNTs were added to 100 mL concentrated HNO_3 (8 M) and then stirred at 60 °C for 4 h, rinsed with tridistilled water several times until the pH value was close to 7. The resulting functionalized MWCNTs was isolated via centrifugation and dried in a vacuum oven at 60 °C for 12 h. The MnO_x–PEDOT coated MWCNTs were prepared as follows: 10 mg functionalized MWCNTs and 4 mmol SDS were dispersed in 10 mL tridistilled water by ultrasonic treatment for 2 h, followed by the addition of 50 μL EDOT to the as-obtained suspension. After stirring for 2 h, 50 mL 6.9 mM $Mn(CH_3COO)_2$ solution was immediately added into the mixture that was followed by stirring of 24 h and then oxidized using 50 mL 4.7 mM $KMnO_4$ solution under stirring. With the oxidation of $KMnO_4$, MnO_x and PEDOT were co-deposited on the functionalized MWCNTs surface. The black solid product was centrifuged and washed repeatedly with absolute ethanol and tridistilled water until the filtrate was colorless, dried in a vacuum oven at 60 °C overnight (denoted as MnO_x–PEDOT–MWCNTs). As a comparison, the PEDOT coated MWCNTs were also prepared with the similar procedure as described above, except using 20 mL 0.2 M $FeCl_3$ solution as the oxidant instead of the $Mn(CH_3COO)_2$ and $KMnO_4$ solutions (denoted as PEDOT–MWCNTs).

To deposit Pt nanoparticles on the MnO_x–PEDOT–MWCNTs support, 40 mg of MnO_x–PEDOT–MWCNTs was dispersed in 100 mL acetic acid buffer (pH = 4) containing $K_2C_2O_4$ (the addition amount of $K_2C_2O_4$ was equimolar with H_2PtCl_6). After ultrasonication for 1 h, 2.65 mL 19.3 mM H_2PtCl_6 solution was added to the suspension. Subsequently, excess $NaBH_4$ (molar ratio of $NaBH_4$/H_2PtCl_6 = 10) was dissolved in 20 mL tridistilled water and put dropwise into the suspension along with continuous stirring at 60 °C for 2 h. The solid catalyst was centrifuged and washed with excess tridistilled water, and then dried under vacuum at 60 °C for later use (denoted as Pt/MnO_x–PEDOT–MWCNTs). Additionally, Pt nanoparticles supported on functionalized MWCNTs (Pt/MWCNTs) and PEDOT–MWCNTs (Pt/PEDOT–MWCNTs) were prepared using the similar procedure as described above.

2.3. Physical characterization

FTIR studies were performed on a WGH-30A model spectrometer (Perkin–Elmer, USA). X-ray diffraction (XRD) patterns were collected using an X-ray diffractometer (Rigaku D/MAX 2500 v/pc, Japan) with a Cu Kα radiation source (λ = 1.5406 Å). X-ray

photoelectron spectroscopy (XPS) measurements were carried out using a Physical Electronics PHI Quantum 2000 system with an Al Kα radiation source, and all reported values of electron binding energy were calibrated with respect to the principal peak of C 1s at 284.5 eV as an internal standard. The morphology and size of the synthesized materials were analyzed by transmission electron microscope (TEM, Philips-FEI Tecnai-F30) with an accelerating voltage of 300 kV. Energy dispersive X-ray (EDX) spectroscopy characterizations were carried out on the same apparatus (Philips-FEI Tecnai-F30). To measure and compare the activity based on the Pt mass, an inductively coupled plasma-optical emission spectrophotometer (ICP-OES, Thermo Electron IRIS Intrepid II XSP, USA) was employed for composition measurements. In this study, The Pt contents of as-prepared Pt/MnO_x–PEDOT–MWCNTs, Pt/PEDOT–MWCNTs and Pt/MWCNTs catalysts were determined to be 19.7%, 19.8% and 14.1%, respectively.

2.4. Electrochemical measurements

The electrochemical measurements were conducted at room temperature around 25 °C on CHI 660D electrochemical workstation using a conventional three electrode cell with a platinum foil (1 cm^2) and a saturated calomel electrode (SCE) as the counter and reference electrodes, respectively. All potentials in the electrochemical tests are quoted versus the SCE scale. The working electrode is prepared as follows: the glass carbon (GC, $\Phi = 5$ mm) electrode, polished with 5.0 μm, 1.0 μm, 0.3 μm Al_2O_3 slurry and washed ultrasonically in tridistilled water, respectively, was used as substrate for the catalysts. Then 3.0 mg of the prepared catalyst and 50 μL Nafion solution (5 wt%) were dispersed ultrasonically in 3 mL tridistilled water, and 15 μL of the suspension was pipetted and air-dried on the pretreated GC electrode at room temperature. For the Pt/MnO_x–PEDOT–MWCNTs, Pt/PEDOT–MWCNTs and Pt/MWCNTs catalysts, the Pt metal loading on the catalyst-modified GC electrodes was 15.06, 15.13 and 10.78 μg cm^{-2}, respectively.

The electrocatalytic performance of catalysts for methanol oxidation was studied in 0.5 M methanol + 0.5 M H_2SO_4 solution. CO stripping voltammograms were obtained by oxidizing pre-adsorbed CO (CO_{ad}) in 0.5 M H_2SO_4 solution at a scan rate of 50 mV s^{-1}. CO was first bubbled into 0.5 M H_2SO_4 for 15 min to allow saturated adsorption of CO onto the catalyst while maintaining the potential at −0.1 V, and then the dissolved CO in the electrolyte was removed by purging with N_2 for 20 min. The amount of CO_{ad} was evaluated by integrating the CO_{ad} stripping peak and correcting for the capacitance of the electric double-layer. The current density in the electrochemical tests was expressed by the normalized current per milligram of Pt loading. Before each electrochemical experiment, the electrolytic solution was purged with pure N_2 for 15 min, and a flux of N_2 was kept over the solution during measurements to prevent the interference of atmospheric oxygen.

3. Results and discussion

3.1. FTIR spectra analysis of nanocomposites

To confirm the presence of PEDOT in the nanocomposites, three supporting materials were characterized by FTIR spectroscopy and the results were shown in Fig. 1. In the case of functionalized MWCNTs (curve a), the spectrum exhibits typical IR absorption of –OH (3440 cm^{-1}) and –COOH (1640 cm^{-1}) stretching vibration [38,39], which is due to the acid oxidation treatment of MWCNTs. As for MnO_x–PEDOT–MWCNTs (curve b), the peaks at 1520 and 1355 cm^{-1} are attributed to the asymmetric stretching mode of C=C and inter-ring stretching mode of C–C in PEDOT, the peaks at

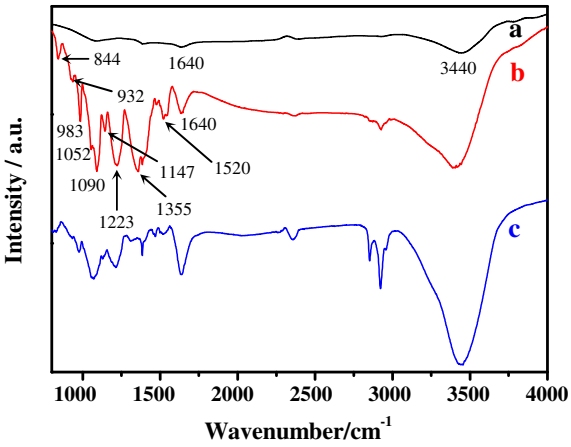

Fig. 1. FTIR spectra of functionalized MWCNTs (a), MnO_x–PEDOT–MWCNTs (b) and PEDOT–MWCNTs (c).

1052, 1090, 1147 and 1223 cm^{-1} are corresponding to the C–O–C bond stretching in the ethylenedioxy ring deformation mode, and the peaks at 844, 932 and 983 cm^{-1} are assigned to the deformation modes of C–S–C in the thiophene ring [40–42]. The spectrum of PEDOT–MWCNTs (curve c) is very similar to that of the MnO_x–PEDOT–MWCNTs. In addition, it is noted that the characteristic peaks of PEDOT in curve b are significantly enhanced as compared to those in curve c, which might result from the interaction of PEDOT with MnO_x. These results indicate that the EDOT was polymerized and successfully coated on the surface of MWCNTs.

3.2. XRD, TEM and XPS characterization of catalysts

The XRD patterns of Pt/MWCNTs, Pt/PEDOT–MWCNTs, Pt/MnO_x–PEDOT–MWCNTs and MnO_x–PEDOT–MWCNTs nanocomposites can be seen in Fig. 2. The (002) peak located at the 2θ value of around 26.1° in all curves evidently originates from the graphite structure of the MWCNTs [12,43]. It is found that the intensity of the (002) peak obviously decreases when containing PEDOT in the composites, which is in agreement with the results of PPy-coated MWCNTs reported in Ref. [13]. For three Pt-based catalysts (curve a–c), the other four peaks at $2\theta = 39.8°$, 46.1°, 67.6° and 81.5° can be ascribed to the diffractions of Pt(111), Pt(200), Pt(220) and Pt(311) planes, respectively, which represent the characteristics of face-centered cubic (fcc) structure of platinum

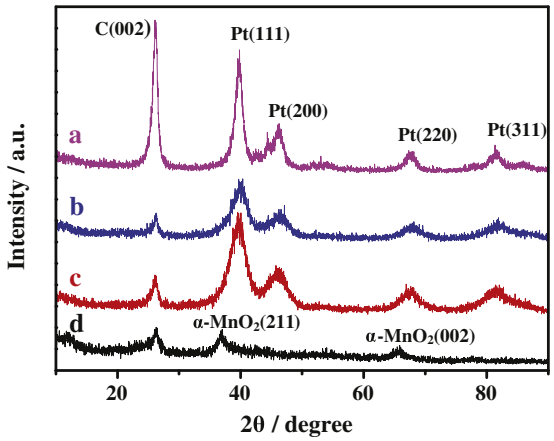

Fig. 2. XRD patterns of Pt/MWCNTs (a), Pt/PEDOT–MWCNTs (b), Pt/MnO_x–PEDOT–MWCNTs (c) and MnO_x–PEDOT–MWCNTs (d).

[4,44]. In the XRD pattern of MnO_x–PEDOT–MWCNTs (curve d), the other two peaks at $2\theta = 36.9^\circ$ and 65.7° are corresponding to the (211) and (002) facets of α-MnO_2, respectively [45,46]. However, the characteristic diffraction peaks of MnO_2 are hardly observed from the XRD pattern of Pt/MnO_x–PEDOT–MWCNTs, which should be due to a small amount of MnO_2 in the composite and the interference of Pt(111) and Pt(220) peaks. Similar XRD results were also reported by others [34]. Moreover, for the Pt/PEDOT–MWCNTs and Pt/MnO_x–PEDOT–MWCNTs, they display significantly broader diffraction peaks than those of Pt/MWCNTs catalyst, suggesting the smaller size of Pt nanoparticles supported on the PEDOT–MWCNTs and MnO_x–PEDOT–MWCNTs. The average crystallite sizes of Pt nanoparticles were estimated by the Scherrer's equation based on the peak assigned to the (220) plane [44]. The (220) plane was chosen for the calculation since this peak does not overlap with other peaks and therefore allows accurate analyses. Therefore, the mean crystallite sizes are determined to be 4.72, 2.37 and 2.42 nm for Pt/MWCNTs, Pt/PEDOT–MWCNTs and Pt/MnO_x–PEDOT–MWCNTs, respectively.

Fig. 3 shows the TEM images of functionalized MWCNTs, PEDOT–MWCNTs and MnO_x–PEDOT–MWCNTs. It can be observed from Fig. 3a that the de-bundled MWCNTs with various diameters are well dispersed and interconnected, generating a maximum nanotube surface area for surface modification. As for the PEDOT–MWCNTs (Fig. 3b), the PEDOT film is homogeneously coated on the surface of MWCNTs, and the nanotubular morphology is retained in this composite. Interestingly, the inclusion of the MnO_x to PEDOT–MWCNTs composite matrix generated different micro-structural features (Fig. 3c), the MnO_x component in the composite is MnO_x nanowire networks, which are closely combined with the PEDOT layer and homogeneously and densely attached on the surface of MWCNTs. The EDX spectrum of MnO_x–PEDOT–MWCNTs (Fig. 3d) shows the peaks corresponding to C, O, S, and Mn elements, confirming the co-deposition of MnO_x and PEDOT on the surface of MWCNTs.

Further investigation on the morphology of as-prepared Pt catalysts was conducted with TEM, and their size distribution was evaluated statistically by measuring the diameter of 200 Pt nanoparticles in the magnified TEM images, as illustrated in Fig. 4. From Fig. 4a and d, the dispersion of Pt nanoparticles on MWCNTs is characterized by a poor distribution with a large number of aggregates. The average particle size of Pt nanoparticles is 4.75 ± 0.5 nm. It is likely due to the non-uniform defects generated on the surface of MWCNTs by the acid oxidation treatment. When Pt nanoparticles are deposited on the MWCNTs surface, the particles tend to deposit on these localized defect sites, thus resulting in the poor dispersion and extensive aggregation. From Fig. 4b and e, Pt nanoparticles are evenly deposited on the surface of PEDOT–MWCNTs with no agglomeration. The average particle size is 2.5 ± 0.3 nm, much smaller than that on the MWCNTs. A possible explanation for this result is that, during the chemical deposition of Pt, $PtCl_6^{2-}$ can be considered as counter ions to dope in the PEDOT matrix. Pt particles can homogeneously distribute on the surface of PEDOT when $PtCl_6^{2-}$ is further reduced [13]. In the case of Pt/MnO_x–PEDOT–MWCNTs (Fig. 4c and f), the average particle size of Pt nanoparticles is 2.5 ± 0.4 nm, which is almost similar to that on the PEDOT–MWCNTs support, indicating that the MnO_x cannot influence the size and dispersion of Pt nanoparticles, but it can greatly improve the electrocatalytic performance of catalyst for methanol oxidation, which will be discussed later.

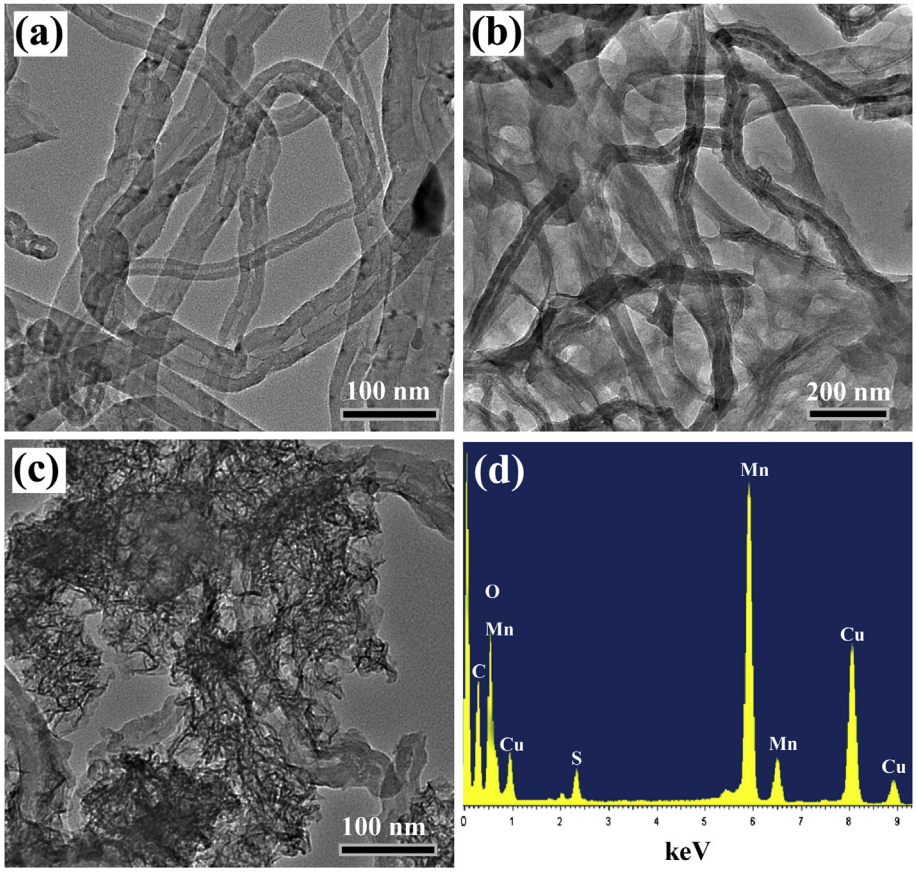

Fig. 3. TEM images of functionalized MWCNTs (a), PEDOT–MWCNTs (b) and MnO_x–PEDOT–MWCNTs (c). (d) EDX spectrum of MnO_x–PEDOT–MWCNTs.

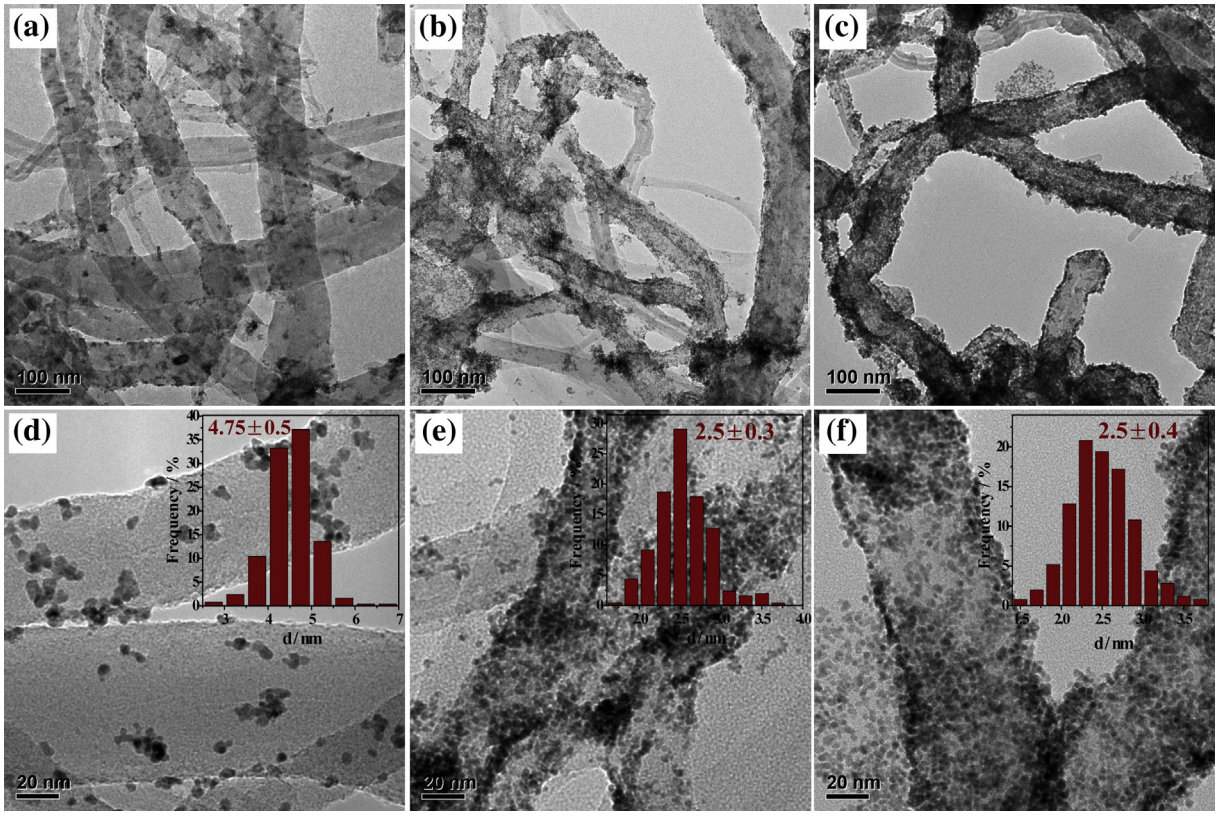

Fig. 4. TEM images of Pt/MWCNTs (a and d), Pt/PEDOT–MWCNTs (b and e) and Pt/MnO_x–PEDOT–MWCNTs (c and f) catalysts, the insets in (d), (e) and (f) are the corresponding size distribution histograms of Pt nanoparticles.

The surface composition and chemical oxidation states of the prepared composites were characterized by XPS. Fig. 5a shows the XPS survey spectra of MnO_x–PEDOT–MWCNTs and Pt/MnO_x–PEDOT–MWCNTs. In the spectrum of MnO_x–PEDOT–MWCNTs (curve A), the signals of C 1s at 284 eV, O 1s at 532.6 eV, S 2p at 170.7 eV and Mn 2p at 643.2 and 654.1 eV can be found, which are consistent with the EDX result. The high resolution spectrum of MnO_x–PEDOT–MWCNTs in Fig. 5b shows that the deconvolution of the highly asymmetric C 1s photoemission yields four peaks at 284.6, 285.9, 286.7 and 288.4 eV due to the C–C of PEDOT and MWCNTs, the C–S and C–O of PEDOT, and the C=O of functionalized MWCNTs [40]. The O 1s signal is composed of three components (Fig. 5c), which involve contributions from different chemical bonds in the composite. The peaks at 529.7, 531.1 and 533 eV correspond to the Mn–O–Mn bond for the tetravalent oxide, the Mn–OH bond for a hydrated trivalent oxide and the H–O–H bond for residual water, respectively [19]. As shown in Fig. 5d, the S 2p region yields two doublets from the spin-orbital splitting of the $p_{3/2}$ (164.6 eV) and $p_{1/2}$ (168.7 eV) states, arising from the PEDOT backbone and from the sulfur in the dopant SDS [40,41]. From the Mn 2p spectrum (Fig. 5e), two main peaks located at 642.1 and 653.8 eV can be assigned to Mn $2p_{3/2}$ and Mn $2p_{1/2}$ of Mn(IV) in MnO_2 [19,34]. Meanwhile, a small quantity of Mn(III) and Mn(V) species also exist. For the Pt/MnO_x–PEDOT–MWCNTs, the Pt 4f spectrum is shown in Fig. 5f, the two pairs of peaks indicate the existence of two different Pt oxidation states on the surface. The peaks of Pt $4f_{7/2}$ at 71.3 eV and Pt $4f_{5/2}$ at 74.6 eV are originated from the metallic Pt(0), while the peaks of Pt $4f_{7/2}$ at 72.4 eV and Pt $4f_{5/2}$ at 75.8 eV are attributed to Pt(II) in the form of PtO or $Pt(OH)_2$ [47–49]. The percentage of Pt(0) and Pt(II) species was calculated from the relative areas of these peaks and it is 68% and 32%, respectively. However, during the deposition of Pt by the $NaBH_4$ reduction procedure, the MnO_2 in the composite might be damaged. Accordingly, the Mn 2*p* signal of Pt/MnO_x–PEDOT–MWCNTs does not appear (curve B in Fig. 5a).

3.3. Electrochemical studies

The electrochemical behaviors of different catalysts were investigated by cyclic voltammetry (CV) measurement, which was performed in 0.5 M H_2SO_4 solution at a scan rate of 50 mV s^{-1}. Fig. 6 shows the CO_{ad} stripping voltammograms of Pt/MWCNTs, Pt/PEDOT–MWCNTs and Pt/MnO_x–PEDOT–MWCNTs catalysts. It can be seen that the onset potential of CO_{ad} electrooxidation on Pt/MnO_x–PEDOT–MWCNTs is 0.13 V, similar to that on Pt/PEDOT–MWCNTs (0.14 V) and much lower than that on Pt/MWCNTs (0.39 V). This result demonstrates that the presence of PEDOT in the catalysts significantly promotes the CO oxidation, but the addition of MnO_x does not enhance the CO oxidation ability of the catalyst, which is consistent with the results of Pt/MnO_2/CNTs reported in the literature [5,34]. Furthermore, the ECSA of catalysts can reflect their intrinsic catalytic activity and the utilization ratio of Pt is closely interrelated with its dispersion situation and the ECSA. Typically, the ECSA can be measured based on H_2 adsorption and desorption or preadsorbed CO electrooxidation. As shown in Fig. 6, the H_2 adsorption/desorption is completely suppressed in the CV curves of the first cycle of preadsorbed CO oxidation, but the peaks associated with H_2 adsorption/desorption appear after the removal of adsorbed CO. The second cycles of preadsorbed CO oxidation are almost overlapped with the stable cycles before CO preadsorption (not shown for concision), which indicates that the H_2 and CO adsorption are in the same Pt active sites. The ECSA based on the H_2 adsorption/desorption charge (Q_H) can be calculated according to the equation of ECSA-H = $Q_H/210(\mu C\ cm^{-2})/W_{Pt}$ [5,34,47]. The

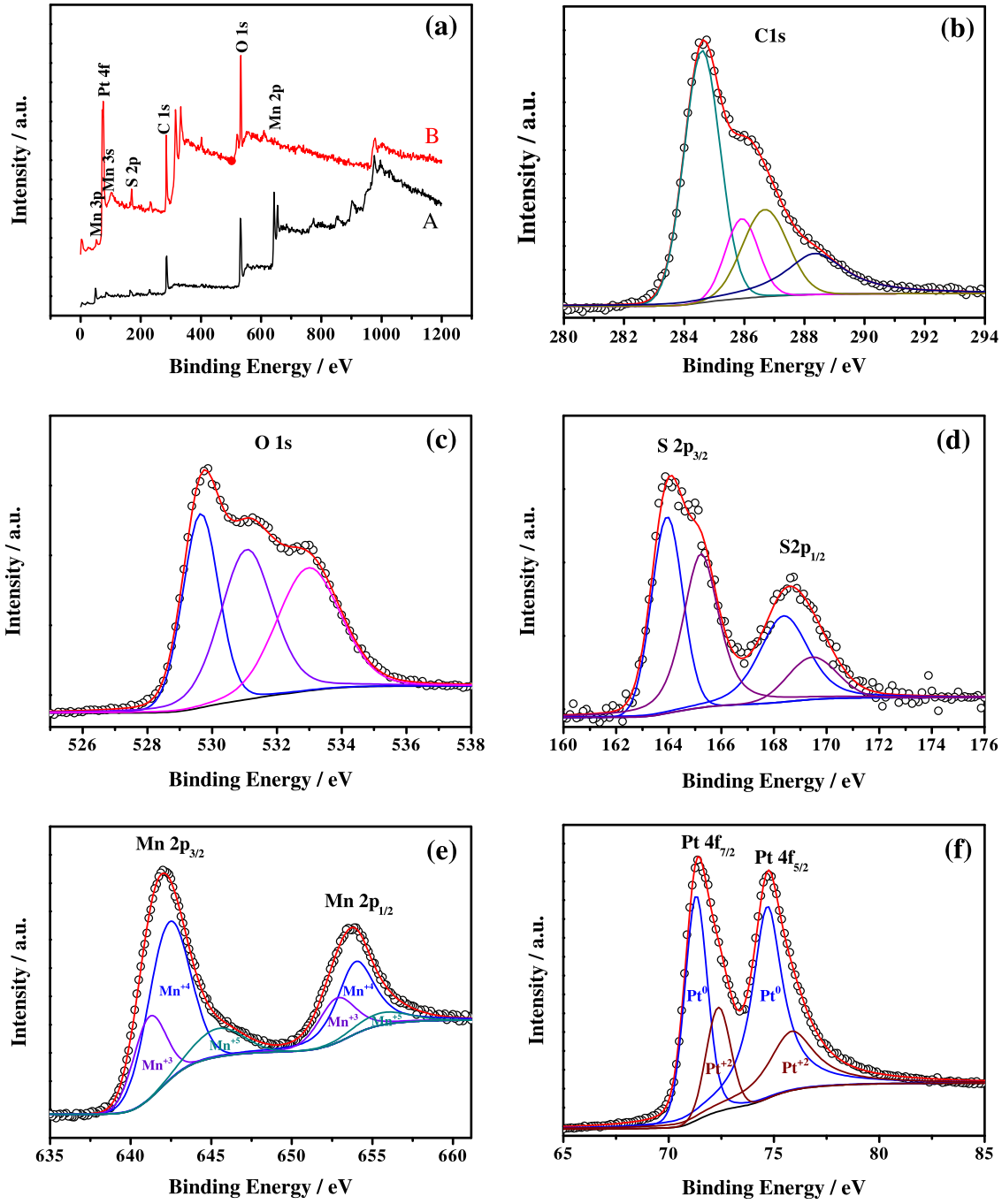

Fig. 5. (a) XPS survey spectra of MnO_x–PEDOT–MWCNTs (A) and Pt/MnO_x–PEDOT–MWCNTs (B). High resolution spectra of C 1s (b), O 1s (c), S 2p (d) and Mn 2p (e) for MnO_x–PEDOT–MWCNTs, and Pt 4f (f) for Pt/MnO_x–PEDOT–MWCNTs.

results are 21.75 m^2 g_{Pt}^{-1} for Pt/MWCNTs, 31.57 m^2 g_{Pt}^{-1} for Pt/PEDOT–MWCNTs and 48.73 m^2 g_{Pt}^{-1} for Pt/MnO_x–PEDOT–MWCNTs. We can also employ the CO_{ad} oxidation charge (Q_{CO}) to calculate the ECSA of the catalysts according to the equation of ECSA-CO = Q_{CO}/484(μC cm^{-2})/W_{Pt} [34,50]. It is 18.02, 22.22 and 39.09 m^2 g_{Pt}^{-1} for Pt/MWCNTs, Pt/PEDOT–MWCNTs and Pt/MnO_x–PEDOT–MWCNTs, respectively. The calculated ECSA-H and ECSA-CO for the three catalysts are comparable, and the Pt/MnO_x–PEDOT–MWCNTs in both cases exhibit much higher ECSA in comparison with Pt/MWCNTs and Pt/PEDOT–MWCNTs. The larger ECSA of the Pt/MnO_x–PEDOT–MWCNTs catalyst might be attributed to the smaller size and better dispersion of Pt nanoparticles and the excellent proton conductivity of MnO_x.

Fig. 7A displays the CV curves of methanol oxidation on Pt/MWCNTs, Pt/PEDOT–MWCNTs and Pt/MnO_x–PEDOT–MWCNTs catalysts in 0.5 M methanol + 0.5 M H_2SO_4 solution. It can be seen that the curves are similar to those reported in the literature [1,23,51], with two irreversible current peaks during the methanol oxidation, attributing to methanol oxidation (forward scan peak at around 0.63 V) and the oxidative removal of adsorbed intermediate species formed in the forward scan (backward scan peak at 0.46 V) [4]. The peak current densities of methanol oxidation on the Pt/MnO_x–PEDOT–MWCNTs catalyst (curve a) in the forward potential scan and in the backward potential scan are 585.1 and 719.7 mA mg_{Pt}^{-1}, respectively, much higher than those on the Pt/PEDOT–MWCNTs (curve b, 357.1 and 441.1 mA mg_{Pt}^{-1}) and Pt/

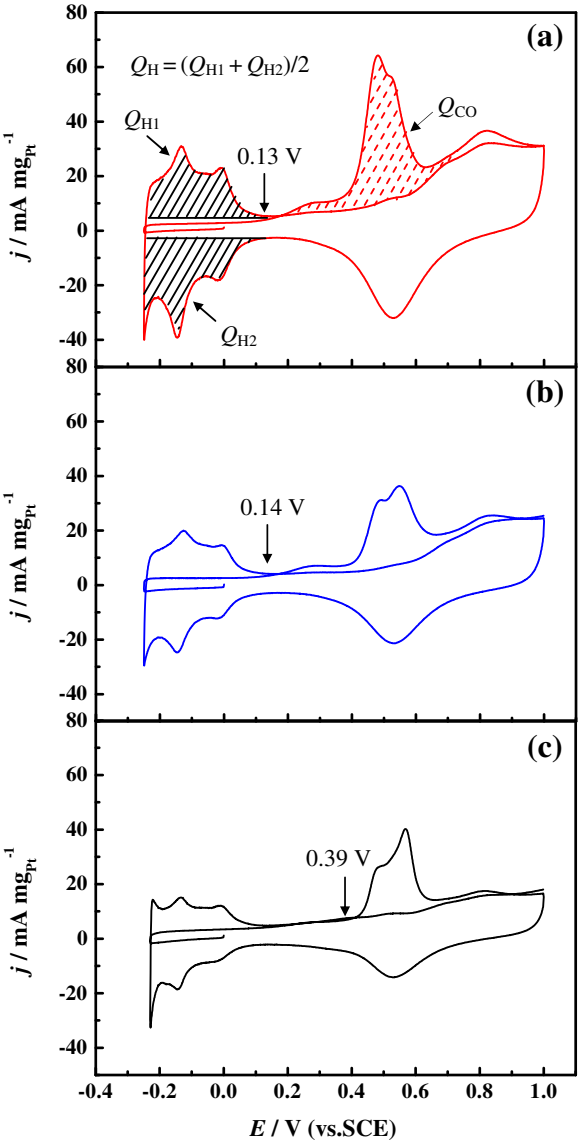

Fig. 6. CO stripping voltammograms of Pt/MnO_x–PEDOT–MWCNTs (a), Pt/PEDOT–MWCNTs (b) and Pt/MWCNTs (c) catalysts in 0.5 M H_2SO_4 solution at a scan rate of 50 mV s^{-1}.

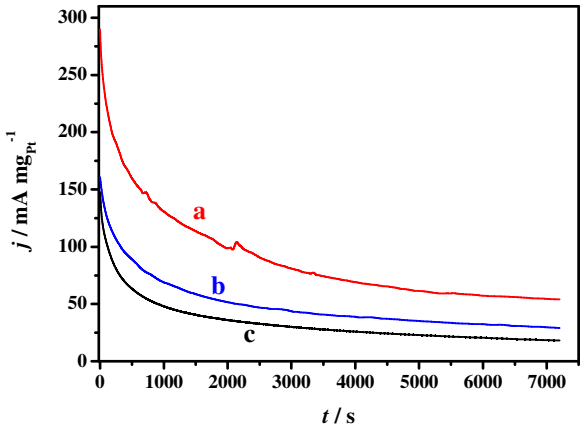

Fig. 8. Chronoamperometric curves of Pt/MnO_x–PEDOT–MWCNTs (a), Pt/PEDOT–MWCNTs (b) and Pt/MWCNTs (c) catalysts in 0.5 M methanol + 0.5 M H_2SO_4 solution at a potential of 0.4 V.

MWCNTs (curve c, 206.8 and 232.3 mA mg_{Pt}^{-1}) catalysts. Additionally, as indicated by dashed lines in Fig. 7B, the corresponding potential for Pt/MnO_x–PEDOT–MWCNTs is 0.27 V at a given oxidation current density (10 mA mg_{Pt}^{-1}), which is shifted negatively by 80 and 110 mV as compared to that for Pt/PEDOT–MWCNTs (0.35 V) and Pt/MWCNTs (0.38 V), respectively. These results demonstrate that the electrocatalytic activity of the Pt/MnO_x–PEDOT–MWCNTs for methanol oxidation is much higher than that of the Pt/PEDOT–MWCNTs and Pt/MWCNTs catalysts. To further investigate the role of MnO_x and PEDOT, the specific activities of the catalysts based on the ECSA were also obtained. As shown in Fig. S1, the specific activity of the Pt/MnO_x–PEDOT–MWCNTs is also higher than that of the Pt/PEDOT–MWCNTs and Pt/MWCNTs catalysts, which indicates that the activity enhancement for methanol oxidation on the Pt/MnO_x–PEDOT–MWCNTs can be attributed to the presence of MnO_x and PEDOT.

In order to compare the long-term electrochemical stability of catalysts in methanol oxidation reactions, the chronoamperometric measurements were carried out in 0.5 M methanol + 0.5 M H_2SO_4 solution at 0.4 V for 7200 s. As shown in Fig. 8, in all current–time curves, the initial current is dropped rapidly in the first 300 s, and then followed by a slower attenuation. The initial fast decay can be ascribed to the formation of intermediate species, such as CO_{ads}, CH_3OH_{ads} and CHO_{ads} during the methanol oxidation reaction [47]. The slow attenuation at longer times is due to the adsorption of sulfate anions on the surface of the catalysts [52,53]. After long-time operation, although the current gradually decays for all the

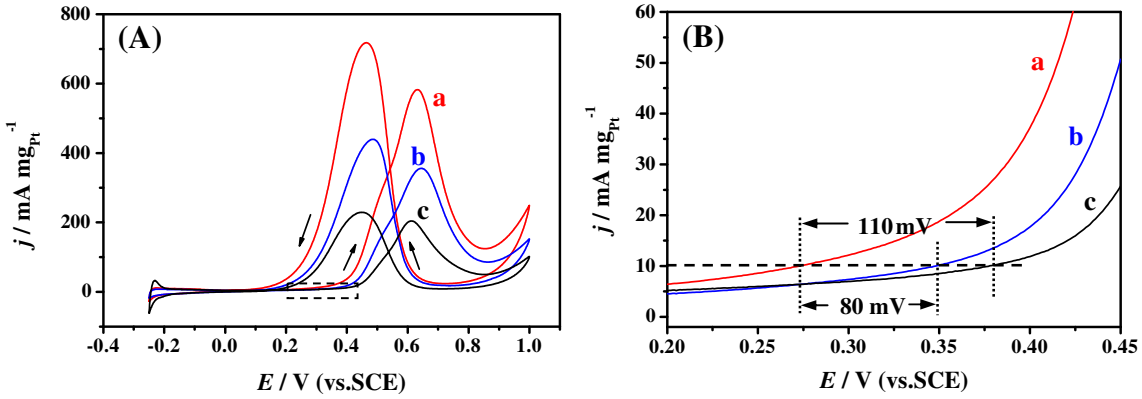

Fig. 7. (A) Cyclic voltammograms of Pt/MnO_x–PEDOT–MWCNTs (a), Pt/PEDOT–MWCNTs (b) and Pt/MWCNTs (c) catalysts in 0.5 M methanol + 0.5 M H_2SO_4 solution with a scan rate of 50 mV s^{-1}. (B) Magnified voltammograms of the boxed area marked in (A).

catalysts, the Pt/MnO_x–PEDOT–MWCNTs maintains a much higher current (curve a), and the final current density is 54.9 mA mg_{Pt}^{-1}, which is almost 1.8 and 3.0 times that of the Pt/PEDOT–MWCNTs (curve b, 30.1 mA mg_{Pt}^{-1}) and Pt/MWCNTs (curve c, 18.5 mA mg_{Pt}^{-1}) catalysts, respectively, indicating that the Pt/MnO_x–PEDOT–MWCNTs catalyst using MnO_x–PEDOT–MWCNTs nanocomposite as the support exhibits more excellent electrocatalytic activity and stability for methanol oxidation. Thus, it can be concluded that the MnO_x in the Pt/MnO_x–PEDOT–MWCNTs brings better electrocatalytic activity and stability for this catalyst. Based on the previous literature [5,34,54], MnO_x in the catalysts could enhance the proton conductivity and the synergetic co-catalytic effect between the Pt nanoparticles and the support, which improve the utilization and electrocatalytic performance of Pt electrocatalysts for the methanol oxidation reaction.

4. Conclusions

In summary, a novel nanostructured electrocatalyst (Pt/MnO_x–PEDOT–MWCNTs) with Pt nanoparticles highly dispersed on the surface of MnO_x–PEDOT–MWCNTs nanocomposite is reported. The structures and electrocatalytic properties of the nanocomposites are characterized by TEM, FTIR, XRD, XPS and electrochemical tests. The hydrogen and CO stripping voltammetry shows the Pt/MnO_x–PEDOT–MWCNTs has the largest ECSA among the three Pt electrocatalysts. The methanol electrooxidation activity and stability of the Pt/MnO_x–PEDOT–MWCNTs are significantly enhanced as compared with the Pt/PEDOT–MWCNTs and Pt/MWCNTs catalysts. Its CO oxidation ability is similar to that of Pt/PEDOT–MWCNTs but largely improved compared with Pt/MWCNTs. The enhanced electrocatalytic performance and utilization of Pt/MnO_x–PEDOT–MWCNTs catalyst can be interpreted by the synergetic interaction of between Pt nanoparticles and MnO_x and the higher proton conductivity of the MnO_x–PEDOT–MWCNTs support. This study may provide a method for the catalytic enhancement of high-performance anodes in DMFCs.

Acknowledgments

This work was supported by the National Natural Science Foundation of China (21263002), Guangxi Natural Science Foundation of China (0991093, 2010GXNSFF013001), and the Foundation Project of Key Laboratory for the Chemistry and Molecular Engineering of Medicinal Resources (Guangxi Normal University), Ministry of Education of China (CMEMR2012-A3).

We are grateful to Professor Shi-Gang Sun for his help in TEM, ICP-OES and XPS characterizations.

Appendix A. Supplementary data

Supplementary data related to this article can be found at http://dx.doi.org/10.1016/j.jpowsour.2013.03.051.

References

[1] S. Patra, N. Munichandraiah, Langmuir 25 (2009) 1732–1738.
[2] J.R.C. Salgado, F. Alcaide, G. Álvarez, L. Calvillo, M.J. Lázaro, E. Pastor, J. Power Sources 195 (2010) 4022–4029.
[3] X.S. An, Y.J. Fan, D.J. Chen, Q. Wang, Z.Y. Zhou, S.G. Sun, Electrochim. Acta 56 (2011) 8912–8918.
[4] J.D. Qiu, G.C. Wang, R.P. Liang, X.H. Xia, H.W. Yu, J. Phys. Chem. C 115 (2011) 15639–15645.
[5] C. Zhou, F. Peng, H. Wang, H. Yu, J. Yang, X. Fu, Fuel Cells 11 (2011) 301–308.
[6] H.S. Liu, C.J. Song, L. Zhang, J.J. Zhang, H.J. Wang, D.P. Wilkinson, J. Power Sources 155 (2006) 95–110.
[7] A. Stein, Z.Y. Wang, M.A. Fierke, Adv. Mater. 21 (2009) 265–293.
[8] Y.K. Zhou, K. Neyerlin, T.S. Olson, S. Pylypenko, J. Bult, H.N. Dinh, T. Gennett, Z.P. Shao, R. O'Hayre, Energy Environ. Sci. 3 (2010) 143–1446.
[9] J. Shi, D.J. Guo, Z. Wang, H.L. Li, J. Solid State Electrochem. 9 (2005) 634–638.
[10] V. Selvaraj, M. Alagar, Electrochem. Commun. 9 (2007) 1145–1153.
[11] H.Y. Wang, F.M. Wang, Y.Y. Wang, C.C. Wan, B.J. Hwang, R. Santhanam, J. Rick, J. Phys. Chem. C 115 (2011) 8439–8446.
[12] H.B. Bae, J.H. Ryu, B.S. Byun, S.H. Jung, S.H. Choi, Curr. Appl. Phys. 10 (2010) S44–S50.
[13] B. Qu, Y.T. Xu, S.J. Lin, Y.F. Zheng, L.Z. Dai, Synth. Met. 160 (2010) 732–742.
[14] C.W. Kuo, L.M. Huang, T.C. Wen, A. Gopalan, J. Power Sources 160 (2006) 65–72.
[15] E. Antolini, E.R. Gonzalez, Appl. Catal. A 365 (2009) 1–19.
[16] E. Frackowiak, V. Khomenko, K. Jurewicz, K. Lota, F. Béguin, J. Power Sources 153 (2006) 413–418.
[17] J. Wang, Y.L. Xu, X.F. Sun, X.F. Li, X.F. Du, J. Solid State Electrochem. 12 (2008) 947–952.
[18] C. Peng, J. Jin, G.Z. Chen, Electrochim. Acta 53 (2007) 525–537.
[19] R.K. Sharma, L. Zhai, Electrochim. Acta 54 (2009) 7148–7155.
[20] T. Abdiryim, A. Ubul, R. Jamal, F. Xu, A. Rahman, Synth. Met. 162 (2012) 1604–1608.
[21] L. Cao, F. Scheiba, C. Roth, F. Schweiger, C. Cremers, U. Stimming, H. Fuess, L.Q. Chen, W.T. Zhu, X.P. Qiu, Angew. Chem. Int. Ed. 45 (2006) 5315–5319.
[22] C.W. Xu, P.K. Shen, J. Power Sources 142 (2005) 27–29.
[23] J.S. Wang, J.Y. Xi, Y.X. Bai, Y. Shen, J. Sun, L.Q. Chen, W.T. Zhu, X.P. Qiu, J. Power Sources 164 (2007) 555–560.
[24] Y. Zhou, Y.F. Gao, Y.C. Liu, J.R. Liu, J. Power Sources 195 (2010) 1605–1609.
[25] K. Ke, K. Waki, J. Electrochem. Soc. 154 (2007) A207–A212.
[26] P. Justin, G.R. Rao, Catal. Today 141 (2009) 138–143.
[27] C.W. Xu, P.K. Shen, X.H. Ji, R. Zeng, Y.L. Liu, Electrochem. Commun. 7 (2005) 1305–1308.
[28] D. Zhang, Z. Ma, G. Wang, K. Konstantinov, X. Yuan, H. Liu, Electrochem. Solid State Lett. 9 (2006) A423–A426.
[29] S. Chen, J.W. Zhu, X.D. Wu, Q.F. Han, X. Wang, ACS Nano 4 (2010) 2822–2830.
[30] P. Lv, Y.Y. Feng, Y. Li, W. Feng, J. Power Sources 220 (2012) 160–168.
[31] S. Komaba, T. Tsuchikawa, A. Ogata, N. Yabuuchi, D. Nakagawa, M. Tomita, Electrochim. Acta 59 (2012) 455–463.
[32] S.R. Sivakkumar, J.M. Ko, D.Y. Kim, B.C. Kim, G.G. Wallace, Electrochim. Acta 52 (2007) 7377–7385.
[33] S.B. Ma, K.W. Nam, W.S. Yoon, X.Q. Yang, K.Y. Ahn, K.H. Oh, K.B. Kim, J. Power Sources 178 (2008) 483–489.
[34] C.M. Zhou, H.J. Wang, F. Peng, J.H. Liang, H. Yu, J. Yang, Langmuir 25 (2009) 7711–7717.
[35] Y.Y. Huang, J.D. Cai, Y.L. Guo, Int. J. Hydrogen Energy 37 (2012) 1263–1271.
[36] R. Amade, E. Jover, B. Caglar, T. Mutlu, E. Bertran, J. Power Sources 196 (2011) 5779–5783.
[37] J. Zhang, J. Jiang, X.S. Zhao, J. Phys. Chem. C 115 (2011) 6448–6454.
[38] G.B. Zhu, X. Zhang, P.B. Gai, X.H. Zhang, J.H. Chen, Nanoscale 4 (2012) 5703–5709.
[39] H.H. Liu, X.J. Huang, B. Gu, Y.K. Choi, J. Electroanal. Chem. 621 (2008) 38–42.
[40] S. Bhandari, M. Deepa, A.K. Srivastava, A.G. Joshi, R. Kant, J. Phys. Chem. B 113 (2009) 9416–9428.
[41] K.R. Reddy, H.M. Jeong, Y. Lee, A.V. Raghu, J. Polym. Sci. Part. A: Polym. Chem. 48 (2010) 1477–1484.
[42] Y.Q. Han, Y. Lu, Synth. Met. 158 (2008) 744–748.
[43] S. Wang, X. Wang, S.P. Jiang, Langmuir 24 (2008) 10505–10512.
[44] Y.J. Li, W. Gao, L.J. Ci, C.M. Wang, P.M. Ajayan, Carbon 48 (2010) 1124–1130.
[45] Z.S. Wu, W. Ren, D.W. Wang, F. Li, B. Liu, H.M. Cheng, ACS Nano 4 (2010) 5835–5842.
[46] C.J. Xu, B.H. Li, H.D. Du, F.Y. Kang, Y.Q. Zeng, J. Power Sources 184 (2008) 691–694.
[47] Y.Q. Huang, H.L. Huang, Y.J. Liu, Y. Xie, Z.R. Liang, C.H. Liu, J. Power Sources 201 (2012) 81–87.
[48] Z.B. Wang, P.J. Zuo, G.J. Wang, C.Y. Du, G.P. Yin, J. Phys. Chem. C 112 (2008) 6582–6587.
[49] H.J. Kim, W.I. Kim, T.J. Park, H.S. Park, D.J. Suh, Carbon 46 (2008) 1393–1400.
[50] A. Pozio, M. De Francesco, A. Cemmi, F. Cardellini, L. Giorgi, J. Power Sources 105 (2002) 13–19.
[51] Y.Y. Chu, Z.B. Wang, Z.Z. Jiang, D.M. Gu, G.P. Yin, Adv. Mater. 23 (2011) 3100–3104.
[52] S. Sharma, A. Ganguly, P. Papakonstantinou, X.P. Miao, M.X. Li, J.L. Hutchison, M. Delichatsios, S. Ukleja, J. Phys. Chem. C 114 (2010) 19459–19466.
[53] G. García, J.F. Montano, A.H. Creus, E. Pastor, G.A. Planes, J. Power Sources 196 (2011) 2979–2986.
[54] K.W. Kim, S.M. Kim, S. Choi, J. Kim, I.S. Lee, ACS Nano 6 (2012) 5122–5129.